Al-Nahrain Journal of Science
ANJS, Vol. 27(5), December, 2024, pp. 123–133

Preparation of A Polymeric Mesh Supported with Nanomaterials to Treat Oil Slick Pollution in the River

Sara S. Hamood[1,*], Majid S. Khalaf[2], Firas S. Mohammed[1]

[1]Physics Department, College of Science, Al-Mustansiriyah University, Baghdad, Iraq
[2]Ministry of Science and Technology, Directorate of treatment of Military, Biological, and Chemical, Disposal, Baghdad, Iraq

Article's Information

Received: 01.08.2024
Accepted: 31.10.2024
Published: 15.12.2024

Keywords:
Zinc oxide,
X- ray photoelectron spectroscopy,
Structure,
Filter,
Polyvinylpyrrolidone.

Abstract

In this project, (ZnO, Ag, ZnO:PVP, Ag:PVP) nanoparticles were synthesized using a pulsed laser ablation method. Various techniques were employed for analyzing and characterizing the nano-products. More, the examination of X-ray technique for oxides indicated possessing Cubic: Cube-like, isometric formation, with a orie predominant orintation sideways (111), (100) and (200). For silver nanoparticles, Zinc oxide and ZnO:Ag NPs respectively. Energy-dispersive X-ray spectroscopy transmission electron microscopy (TEM) analysis, X-ray fluorescence (XRF), Fourier-transform infrared spectroscopy, and photoluminescence measurements (PL) were among them. Membrane purification techniques are currently extensively utilized in environmental uses, such as water and wastewater treatment, as well as in various industries including agri-food and biotechnology. the study incorporated the use of polymer-supported nanomaterials, with PVP selected for its excellent chemical and thermal resistance. Various membrane structures with differing porosities were prepared and effectively employed for the filtration of oil-polluted water, as validated through TEM, XRF, and other measurements. In this context, the polymer functioned akin to a sponge for water pollution remediation.

http://doi.org/10.22401/ANJS.27.5.14
*Corresponding author: sarasameer@uomustansiriyah.edu.iq

1. Introduction

Due to large scale of petrochemical process uprising, refineries and transportation , water pollution is a remarkable issue has been emerged.[1] the main resources of these wastes or water pollution is petrochemical and gas oil factories.The oil compounds that is mixed with water resulted from these industries may consist of many compounds and parameters.[2-5] From one perspective, petroleum output comprises volatile organic chemicals (VOCs)& extra noxious plus detrimental constituents, that potentially able to impact the generation and development of marine life. [6-7] The significant quantity of oily wastewater can diminish the productivity and varity of marine life. Harmful substances in oily wastewater can lead to environmental disruptions, such as modifications to the aquatic ecosystem and disruption of feeding hierarchies. Specifically, compounds plus poisons that gather during the base of the feeding hierarchies & are then transferred towards human through ingesting can origin severe health issues. Moreover, toxic substances can have multiple harmful effects on the Adjacent area, such as air contamination from disappearance of lubricant besides Carbon-based materials into the environmental envelope. They can also influence marine water and potable water. Additionally, a significant oil spill on the ocean's surface may result in fires and jeopardize maritime safety.[8] The factors contributing to this situation include not only the crew's insufficient safety awareness, inadequate oversight, and other administrative flaws, but also the absence of efficient and cost-effective methods for managing marine oily wastewater. To minimize the outflow of petroleum-contaminated waste from vessels and lessen marine contamination, it is crucial to enhance technologies for marine oily wastewater treatment while also reinforcing ship supervision. In recent years, substantial advancements have been achieved in

marine oily wastewater treatment technology, driven by the efforts of scientists globally. [9] Nanotechnology is a burgeoning and hopeful field with potential applications in consumer items, industrial domains, and medical products. [10] The risk of human and environmental exposure to nanoparticles is rising as the scope of applications broadens. Their possible Harmful impacts persist being studied, the comprehension of the impact of contrived nanoscale contaminants within life framwork being currently limited. [11- 12]. Owing to their considerably larger surface area, nanoparticles are far more reactive than bigger particles. Furthermore, they exhibit unique chemical and physical characteristics. [13- 16] Numerous metallic and metallic oxide nanoparticles, like (Ag), (Ag_2O), (TiO_2), (ZnO), (Au), (CaO), (Si), (CuO) and (MgO), showed to exhibit antimicrobial activity. [13] The human body requires metals, also known as metal ions, for more than 300 various enzymatic functions. [17-20] PVP is a moisture-absorbing polymer that dissolves easily in water and is compatible with biological systems. [21] Polyvinylpyrrolidone exhibits outstanding moistening characteristics, which is why it's commonly used in the medicinal and health sectors. Other uses include personal care items, paints, adhesives, and as a food additive. Current non-pharmaceutical research on PVP is concentrating on PVP adsorption onto particles, cross-linking, the creation of new PVP-based polymers, and the properties of PVP mixtures. [22-23] Membrane methods of filtration are frequently employed in the environmental disciplines of water and wastewater treatment, as well as in businesses such as agriculture, food processing, and biotechnology. The extensive use of polymeric membranes is due to their inexpensive manufacturing costs and ease of managing huge surface areas. Polyvinylpyrrolidone (PVP) is a popular polymer for microfiltration and ultrafiltration membranes due to its excellent chemical and thermal stability throughout a wide pH range. [24–26] PVP also acts as a Pore-generating substance in membrane production via phase transformation. Subject to the polymer's attributes and the ratio of polymer additive, it's possible to create film layers with different morphology forms and hydrophilicities, which in turn results in varying performance regarding permeability, rejection, or fouling resistance. [27–30].

2. Materials and Methods

PLAL (Pulsed Laser Ablation in Liquid) was employed to produce various nanoparticles, including ZnO, Ag, Ag:PVP, ZnO:PVP, ZnO:Ag:PVP, and Ag:ZnO, in deionized water. The process involves a two-step method: First, a high-purity metal plate is submerged in 1.5 mL of deionized water in a glass container and irradiated with an Nd:YAG laser (1064 nm wavelength, 8 ns pulse duration, 2 Hz repetition rate, 420 mJ per pulse), using a converging lens with a 100 mm focal length to focus the beam. To produce Ag:ZnO nanoparticles, a 2-mm-thick silver plate is ablated for 60 minutes, followed by ablation of a zinc plate onto the silver colloids for another 60 minutes. Polyvinyl pyrrolidone (PVP) is commonly used as a template in this process. PVP (polyvinylpyrrolidone) is super versatile and can be dissolved in a bunch of organic solvents or water. It not only boosts the viscosity of the spinning solution but also impacts the creation of ZnO:Ag nanoparticles (NPs) using the PLA (Pulsed Laser Ablation) method.

For comparison, Ag NPs or ZnO NPs are made using a laser ablation technique on a silver or zinc plate, respectively, in deionized water for 60 minutes. To prepare the ZnO:Ag, ZnO, and Ag NPs, 10 grams of PVP is dissolved in deionized water in a round-bottom flask with continuous stirring at room temperature (23 °C) for at least 20 minutes, until the polymer is fully melted. This process is then repeated to get the desired nanoparticle compositions. Distinct densities of nanoparticle solutions (one, ten, and hundrad mg per liter) has been assembled using highly refined water and diffused in an ultrasonicator for 20 minutes. Fresh suspensions were made before each experiment. Since nanoparticles fully integrated at pH 6 and 12, experiments have implemented within a pH spectrum of seven to eleven .

For the filtration study, the membrane had been thoroughly washed with distilled water after every 60 mL batch. Real river water was used for testing. The film permeate flux (L/m^2h) and nanoparticle rejection (%) were measured over distinct time periods employing stirred ultrafiltration cells. Membranes with varying molecular weight cutoffs (PES: 10,20, 30,50 and 100 kDa) were screened for layer permeability and ZnO preservation. The PES of twenty kDa membrane (P020F) has been designated for further studies. The impact of alkalinity (200 mg/L) and natural organic matter (NOM), represented as humic acid (2 mg/L), on ZnO suspension was examined. Such densities were chosen to mimic natural river water conditions. Results are presented as the mean value from three distinct experiments. film permeate flux and rejection were calculated using specified equations, and flux normalization was performed accordingly.

$$\text{Membrane flux } (\text{L/m}^2\text{h}) = \frac{(\text{Permeate volume, L})}{(\text{membrane area, m}^2 \times \text{time, h})} \quad (1)$$

$$\text{Flux normalized } (J/J_0) = \frac{\text{Permeate flux } (J)}{\text{Pure water flux } (J_0)} \quad (2)$$

$$\text{Retention } (\%) = \frac{\{(C_f - C_p) \times 100\}}{C_f} \quad (3)$$

where C_f = Feed ZnO concentration, C_p = Permeate ZnO concentration.

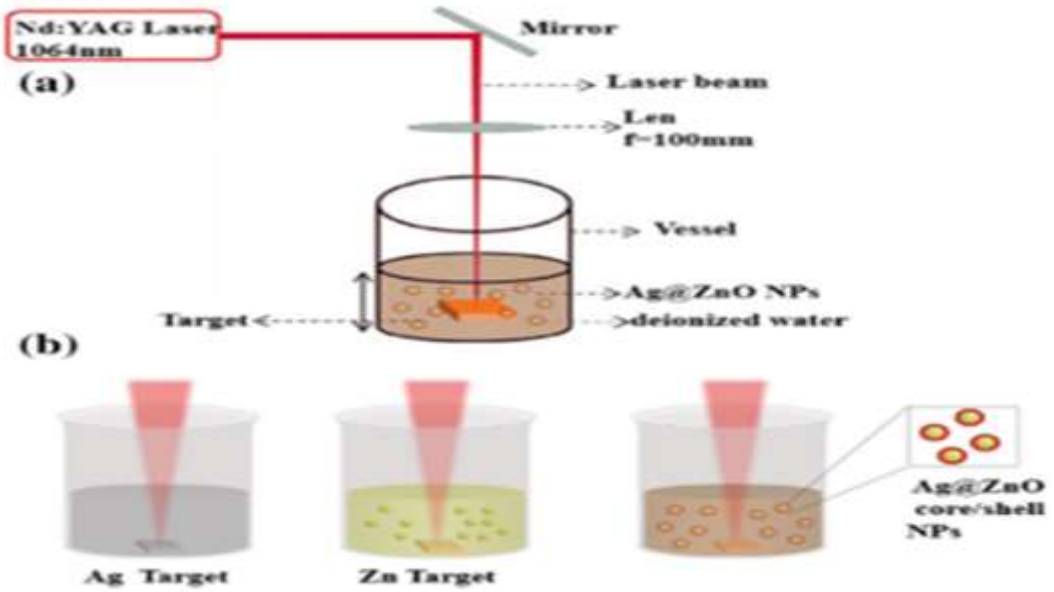

Figure 1. a Schematic diagram of the PLAL setup. b Synthesis process of the ZnO:Ag nanostructures.

3. Results and Discussion

3.1. X-ray diffraction

The nanoparticles (NPs) can be identified using the X-ray diffraction (XRD) patterns illustrated in Figure 2. Figure 2A displays the XRD pattern of silver nanoparticles (Ag NPs). The XRD intensities observed at 2θ angles of 38.46°, 44.43°, 64.57°, 77.5°, and 81.39° correspond to the crystalline planes (111), (200), (220), (311), and (222) of Ag NPs, correspondingly. The obtained intensities crests align with the data provided in the JCPDS file card 04-0783, which represents the face-centered cubic structure of silver.In Figure 2B, the black curve reveals six peaks located at 31.8°, 34.5°, 36.3°, 47.6°, and 56.75°. These peaks are assigned to the crystalline planes (100), (002), (101), (102), (110), and (103) of zinc oxide nanoparticles (ZnO NPs), correspondingly. The whole XRD data peaks of ZnO nanoparticles (ZnO NPs) correspond to the hexagonal wurtzite structure of ZnO (JCPDS card no. 36-1451). This indicates that the ZnO NPs possess excellent crystal quality. The red curve in Figure 2B shows the XRD trace for the Ag: ZnO0 core–shell nano compasites. It reveals two sets of diffraction peaks, corresponding to both Ag and ZnO. These peaks match the face-centered cubic structure of silver

(JCPDS card no. 04-0783) and the hexagonal wurtzite structure of ZnO (JCPDS card no. 36-1451). Relative to the diffraction traces observed in Ag NPs and ZnO NPs, there is no significant shift in the diffraction peaks of Ag and ZnO in the Ag:ZnO NPs. Certainly, Here's the passage with synonyms substituted. The lack of impurity peaks indicates the high purity of the Ag:ZnO core–shell nanostructure produced through liquid-phase laser ablation. As the concentration of Ag increased, the peak intensity of the Ag phase in the nanocomposites became more pronounced and sharper, suggesting that metallic Ag deposits on the ZnO nanoparticle surfaces rather than integrating into the ZnO lattice. The consistent peak positions confirmed that Ag particles resided on the surfaces of well-crystallized ZnO nanoparticles. Moreover, the crystallite size of the Ag–ZnO nanocomposites, as determined using the Scherrer equation, expanded from 12 nm to 20 nm with higher Ag levels, attributed to Ag nanoparticles adhering to the ZnO surfaces [31]. The crystallinity of the composites, the average crystallite size of mostly NPs was calculated using the Debye-Scherrer equation after successful synthesis. The Scherrer equation is the basic and most widely used equation for calculating crystallite size by combining 2θ and FWMH values from XRD data [32].

$$D = \frac{K\lambda}{\beta} COS\theta \quad \ldots (4)$$

In this equation, D represents the crystallite size (diameter), K is Scherer's constant (0.9), λ = 0.15406 nm (the wavelength of the X-ray source), β represents the full width at half the maximum intensity (FWHM) in radians and θ is used to indicate the positions of the peaks are in (radians), which is the Bragg angle of diffraction for the relevant XRD peak.

Table 1. The obtained result of the XRD for ZnO, Ag and ZnO:Ag Nanomaterials

ZnO NPs			
2θ(Degree)	(hkl)	d(nm)	FWHM
31.8634	100	39.978717	0.20657
34.52717	002	38.595684	0.21546
36.35097	101	39.438605	0.21193
47.66288	102	35.3160305	0.24582
56.71602	110	34.04042632	0.2651
Ag NPs			
2θ(Degree)	(hkl)	d(nm)	FWHM
38.24551	111	12.45995169	0.67012
44.28944	200	10.03220178	0.8295
64.54923	220	12.67446047	0.73338
77.46468	311	13.9153946	0.72494
81.48946	222	29.7356351	0.35184
ZnO:Ag NPs			
2θ(Degree)	(hkl)	d(nm)	FWHM
31.83879	100	38.43881028	0.19867
34.51281	002	37.32337393	0.20319
36.32963	101	36.42146579	0.20717
39.09744	111	46.92402287	0.15948
43.28705	200	40.40791347	0.18267
47.63779	102	30.73623269	0.23636
56.6809	110	26.40991021	0.26465

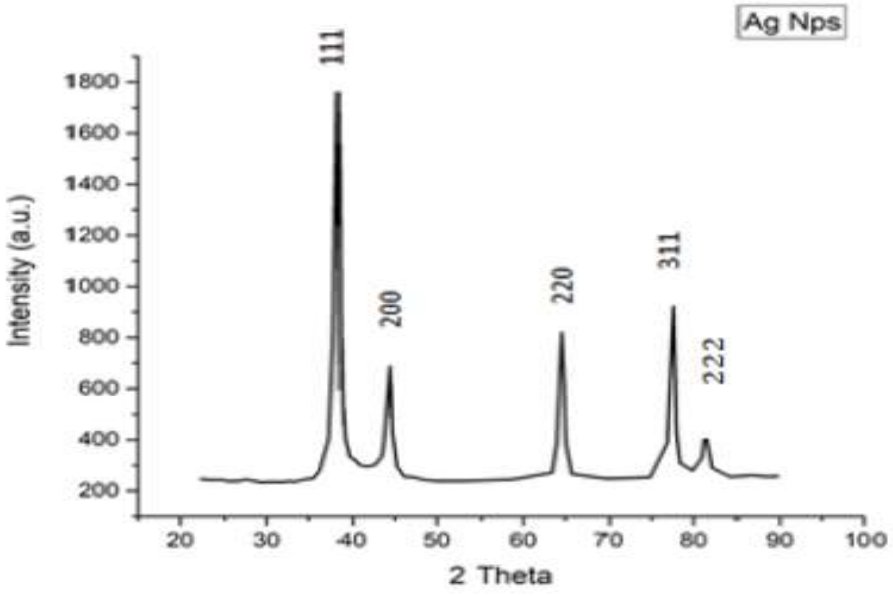

(a)

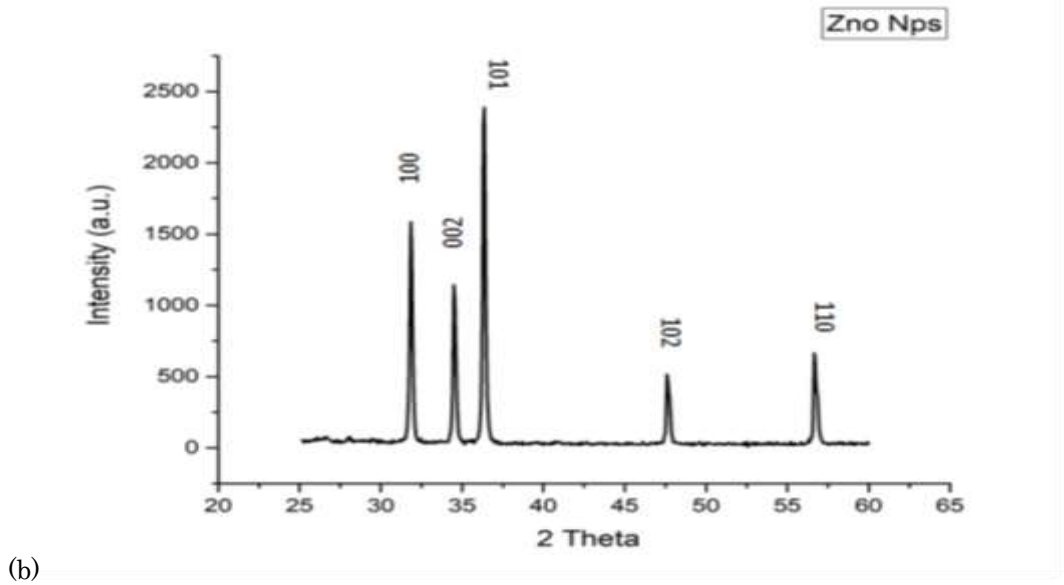

(b)

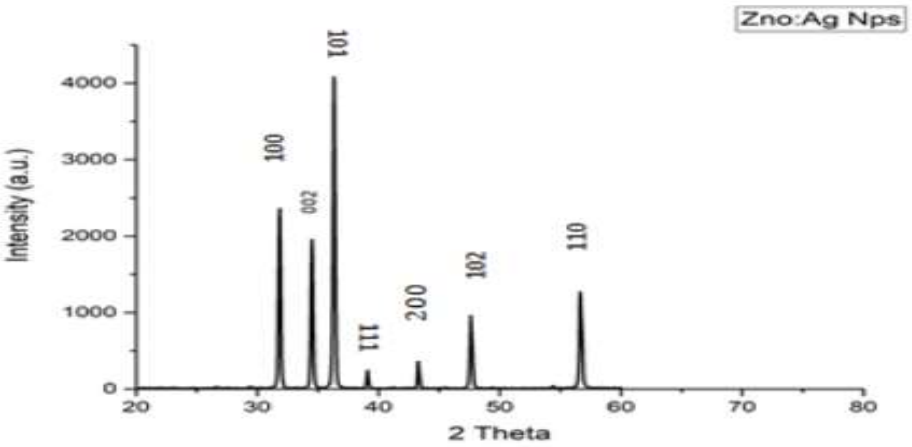

(c)

Figure 2. XRD patterns of (a) Ag, (b) Zno, and (c) ZnO: Ag NPs

3.2. Fourier transformation infrared spectroscopy (FTIR):

The identification of functional groups is greatly aided by FTIR spectroscopy. ZnO absorption band is depicted in Figure 3, where peaks are found at 1644.30, 2954.43, 2895.97, and 3392.86 cm−1, which represent the C=O, CH, and NH groups, respectively. Ag NPs' FTIR absorption spectra show large NH absorption-related absorption peaks at 3391.48 and 3307.46 cm−1. The extended vibrations at 3273.30 cm−1 correspond to amine (OH) groups, while the band at 1644.71 cm−1 relates to C=O stretching modes. The spectra also show C–H stretching (alkanes) and O–H stretching (alcohols) at 2965.42 and 2920.27 cm−1. Comparably, ZnO: Ag NPs' FTIR absorption spectra reveal that NH stretching (amines) occurs at around 3393.38cm−1, whereas C–H stretching (alkanes) is found at 2964.44cm−1. Regarding Ag: ZnO, a strong band at 493 and 428 cm−1 is ascribed to vibratory ZnO elongation and deformation, respectively, whereas an absorption band at 1644.13 cm−1 suggests C=O stretching.

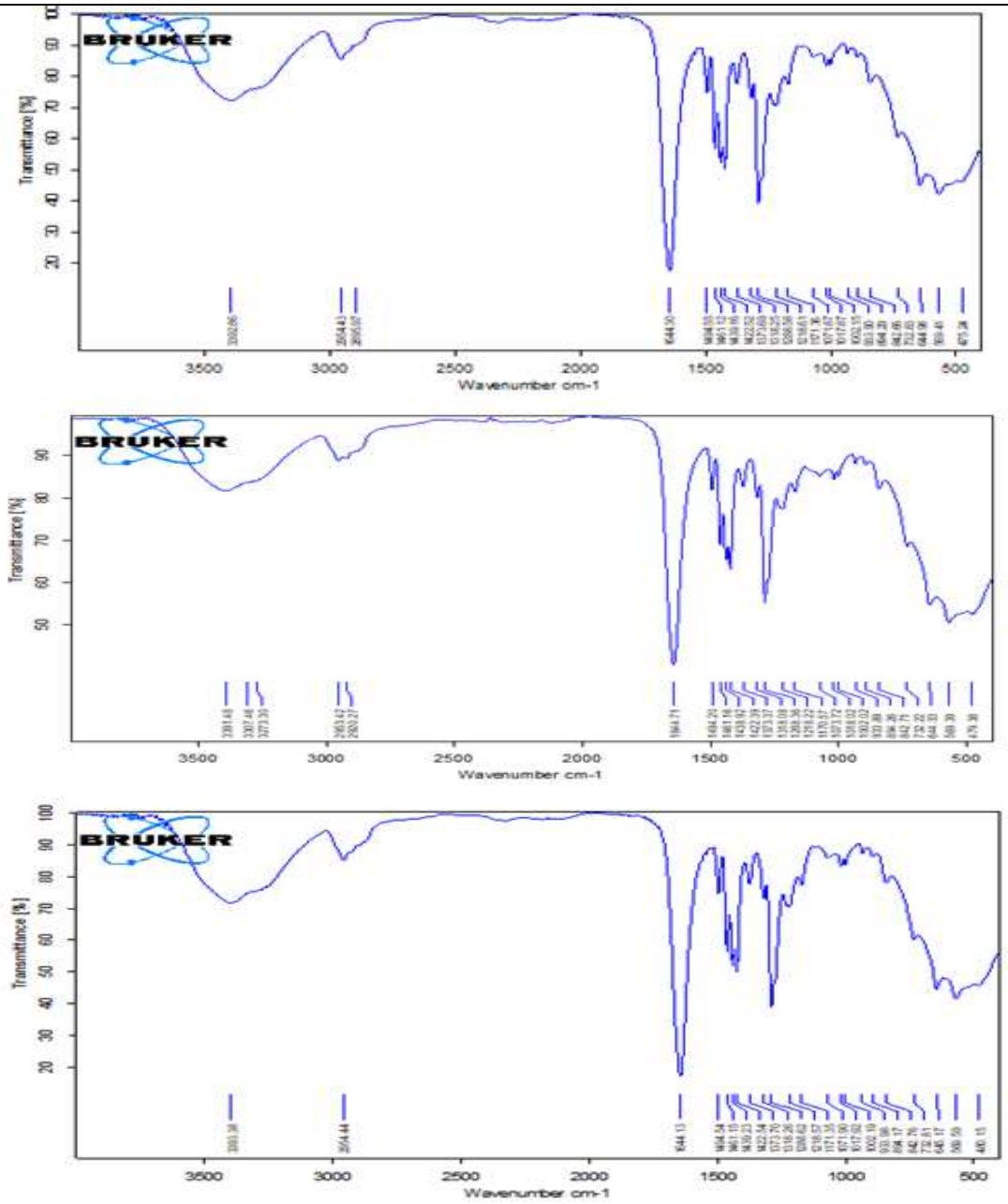

figure 3. FTIR of Zinc oxide, silver and mixture of Zinc oxide and sliver nanoparticles.

3.3. Photoluminescence measurements (PL)

Figure 4 displays the room temperature photoluminescence (PL) spectra, presenting sharp emissions within the UV spectrum (~380 nm) and broad bands in the visible light range (~580 nm). The UV emission is attributed to band gap transitions, whereas the visible emission is attributed to defects - related combining of holes and electrons surrounded at oxygen vacancies in ZnO. Figure 5 presents PL measurements as a function of wavelength for undoped ZnO nanoparticles (NPs), Ag NPs, and Ag-doped ZnO NPs, assembled via laser ablation in water at room temperature.Figures 4-A, B, and C display the emission wavelengths for ZnO at 430 nm, Ag at 485 nm, and ZnO at 440 nm. These emissions correspond to the recombination processes between electrons and holes generated by photon emission. The increase in electron concentration, due to silver doping and the presence of crystal defects from oxidation processes during the laser ablation deposition in water, influences these emission wavelengths. Notably, the photoluminescence (PL) intensities for defect emissions are consistently enhanced. This suggests that the embedded Ag

nanoparticles significantly affect both the band gap and the defect emissions of the ZnO films.

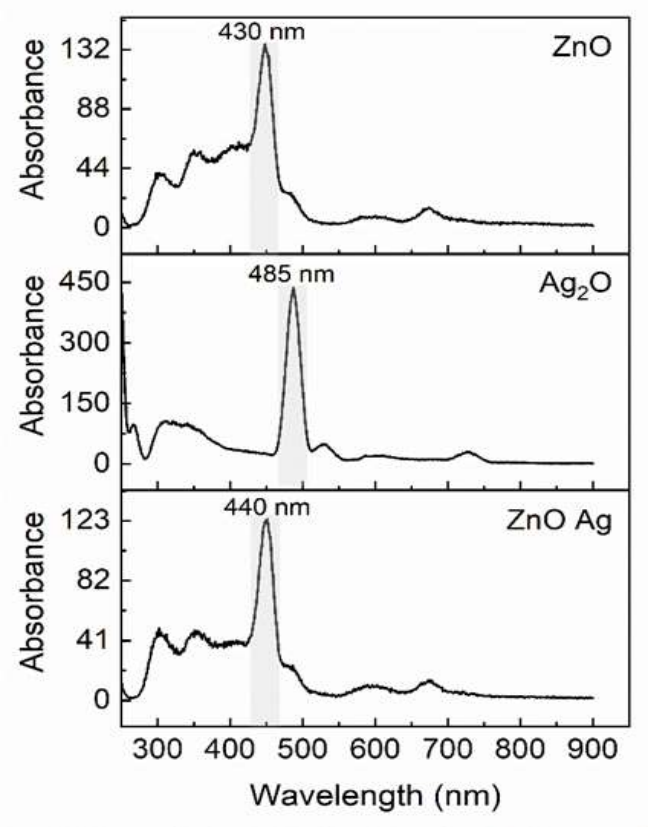

3.4. Transmission Electron Microscopy (TEM)

TEM images showing the formation of ZnO nanoparticles, Ag nanoparticles, and mixed ZnO:Ag nanoparticles with PVP, along with filters for each, are presented. The average size of the nanomaterial is under 50 nm. Figure (5) displays a TEM micrograph that clearly shows a spherical shape and a narrow size distribution of the particles. This dispersible material was analyzed under TEM, even at high magnification, but crystallization could not be determined. With minimal aggregation, some of the nanoparticles and nanosheets appeared to have an uneven shape.

3.5. X-ray photoelectron spectroscopy (XPS) analysis

XPS analysis has been carried out to explore the chemical form and formation of the surface for Silver-Zinc Oxide Nanoparticles, which is crucial for Photocatalytic efficiency. The traces depicted in Figure 6a confirmed that the Ag–ZnO nanoforms exhibit elemental signals from C, O, Zn and silver Ag atoms, consistent with the XRD results. Figure 6 displays the XPS spectra of Ag–ZnO nanocomposites: (a) the survey spectrum, (b) the Zn2p3 spectrum, and (c) the Ag3d spectrum. No additional non-essential elements have been detected, in advance, the high level of nanocomposites purity. C - intensity (not shown) at C 1s = 284.8 eV is attributed to residual carbon from the sample and hydrocarbons from the XPS instrument. The fine-dispersed spectra of Zn 2p, O 1s, and Ag 3d are shown in Figure 3b–d, with the binding energies of nanocomposites varying considerably, indicating strong interactions between the Ag and ZnO nanoparticles. Figure 3b reveals a peak at 1022.06 eV corresponding to Zn 2p3/2, indicating a normal state of Zn^{2+} in the Ag–ZnO nanocomposites, and another peak at 1044.4 eV, representing the binding energy of Zn 2p1/2 (see Figure 3a). The core-level spectrum (see Figure 3a) reveals two distinct sub-crests at 532.43 eV (O I) and 530.95 eV (O II). In the XPS spectrum, the peak at the higher bond energy (O I) is associated with adsorbed oxygen or hydroxide, while the crest at the lower binding energy (O II) corresponds to lattice oxygen in the Ag–ZnO nanocomposites. During the photocatalytic process, surface hydroxyl groups play a significant role. Figure 3d Presents the Ag 3d high-resolution spectrum, which is deconvoluted into three peaks. The peaks at 374.6 eV and 368.6 eV are attributed to Ag $3d_3/_2$ and Ag $3d_5/_2$, respectively, for metallic silver (Ag^0). This confirms the successful decline of Ag ions to metallic silver in the Ag–ZnO nanoformation.

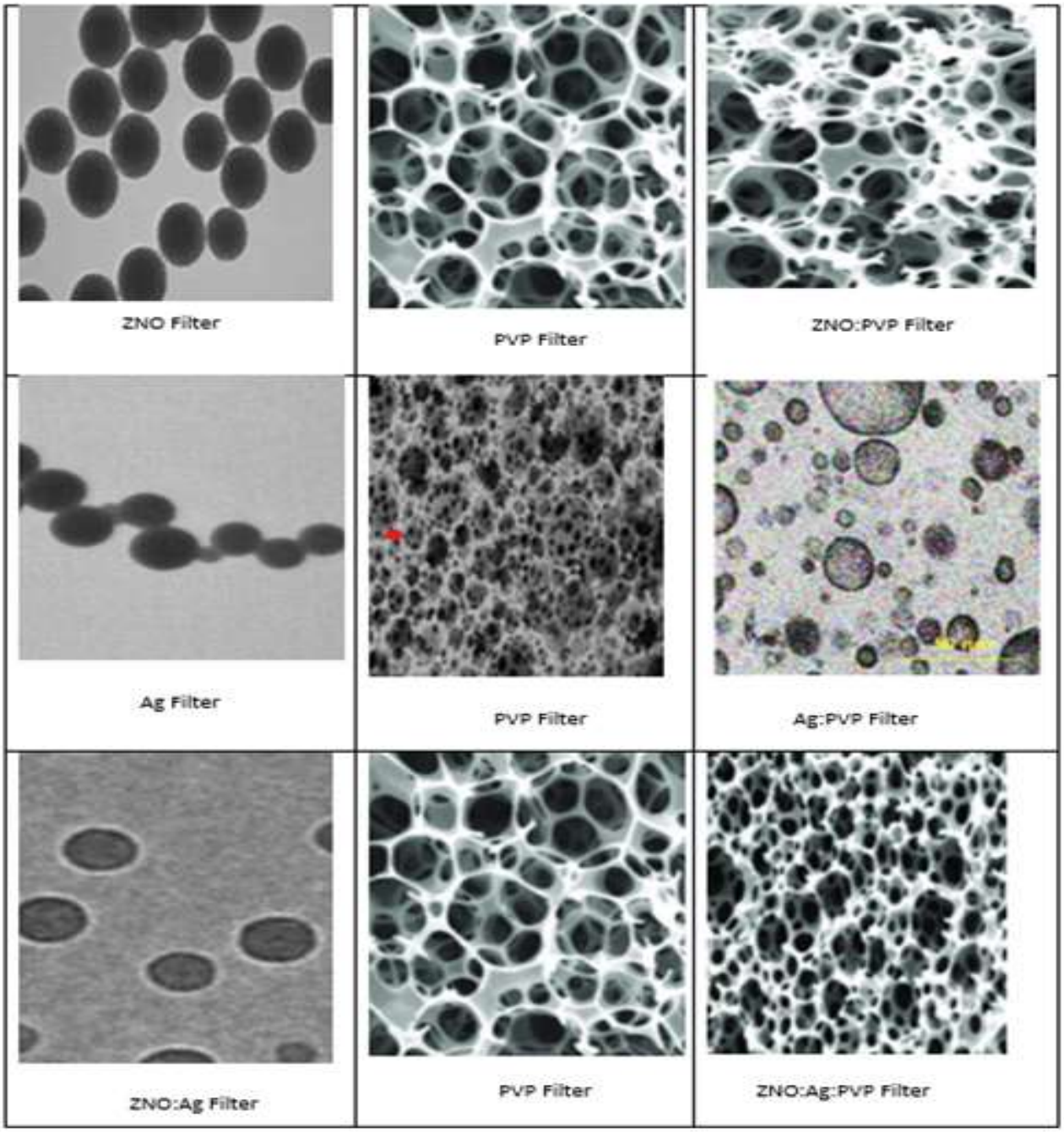

Figure 5. TEM images of nanocrystal formation of ZnO NPs Filter, Ag NPS Filter, and Zno : Ag NPs Filter ,PVP Filter ,Zno:Ag:PVP Filter , ZNO:PVP Filter , Ag:PVP Filte

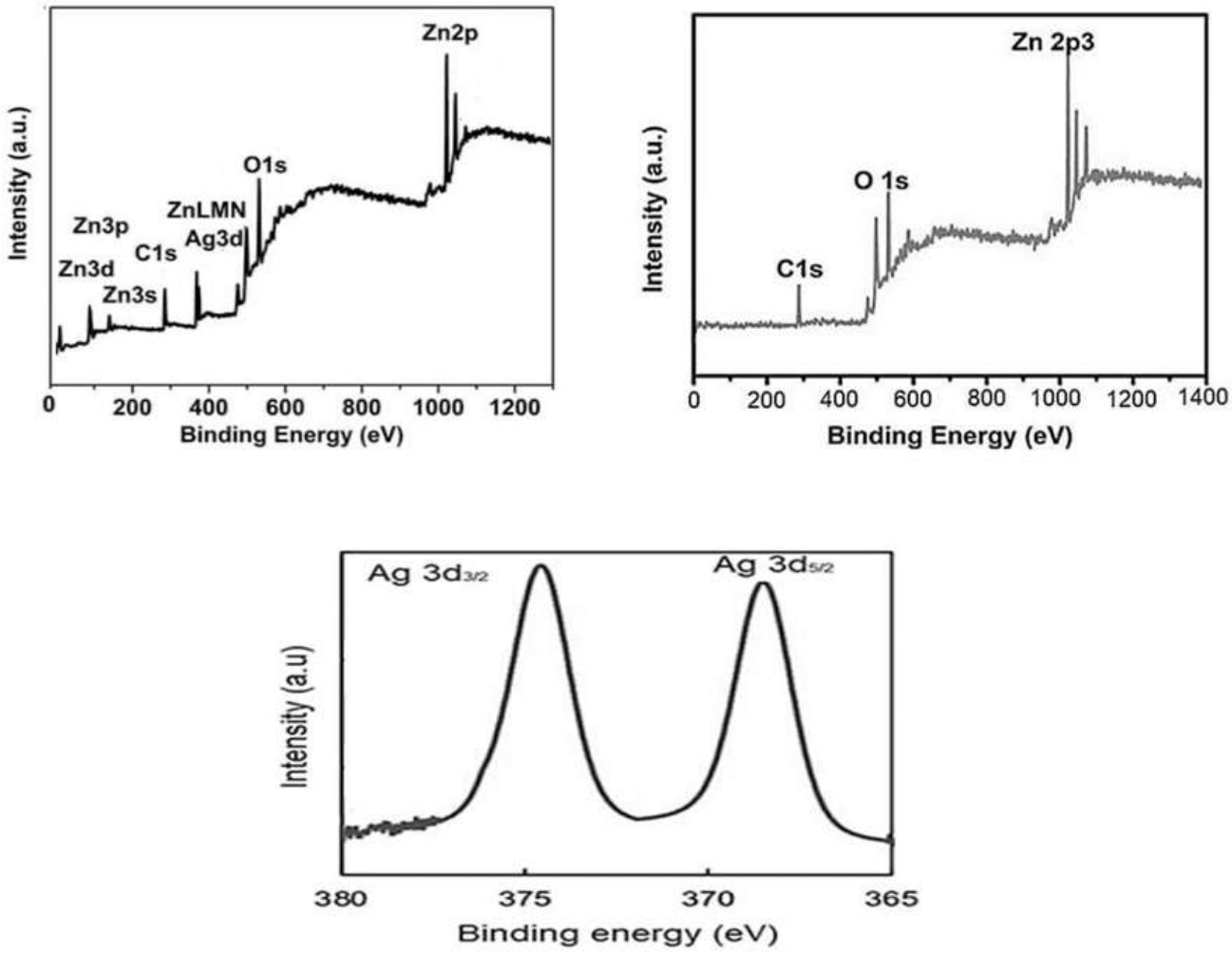

Figure 6. XPS spectra of (a) ZnO:Ag (b) ZnO, (c) Ag nanoparticles.

3.6. X-ray Fluorescence Spectroscopy:

The proportions of elements in water contaminated with oil and other substances were measured after the filtration process. Table 4-5 presents the X-ray fluorescence (XRF) results for the oil-contaminated water. The table indicates that the water contains several elements, including carbon, phosphorus, phosphate, silver, potassium, iron, sodium, and magnesium, with carbon being present in the highest percentage. Another table shows the elemental composition of the water after the filtration process.

The chemical formula of the oil is:

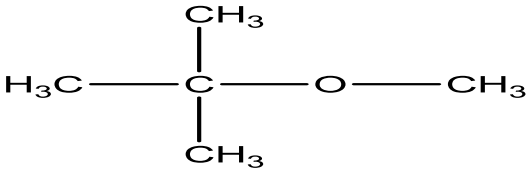

Table 2. The XRF for polluted

Elements	Wt. (%)			
	Mineral Oil and after filtration	***Mineral Oil after ZnO/Flitter***	***Mineral Oil after Ag/Flitter***	**Mineral Oil after ZnO:Ag/Flitter**
C	12	10	9	3
O	5	3	9	10
B	8	3	2	-
Fe	70	40	20	36
P	0.4	0.1	-	-
Ca	0.5	0.4	0.3	-
Cr	-	0.3	0.1	-
Zn	-	1.0	1.2	1.1
Ce	-	-	-	0.1

4. Conclusions

ZnO, Ag, and ZnO: Ag NPs were successfully synthesized, with and without PVP, using the laser ablation method. These NPs were explored for their potential applications in environmental purification. Analysis via XRD patterns revealed sharp peaks, indicating the absence of impurities in the prepared samples. SEM images depicted uniformly shaped particles for Ag, ZnO, and ZnO: Ag NPs. Measurements conducted before and after using the nanomaterials yielded promising results, highlighting the efficacy of PVP as it functioned akin to a sponge for pollutants present in water. By varying polymer properties and the additive-to-polymer ratio, membranes with diverse morphologies (pore structures) and hydrophilic properties can be finely tuned, influencing performance factors such as permeability, rejection rates, and resistance to fouling.

Conflict of Interest: The authors declare that there are no conflicts of interest.

Funding: No funds have been received for this work.

References

[1] Alarifi, S.; Ali, D.; Verma, A.; Alakhtani, S.; Ali, B. A.; "Cytotoxicity and genotoxicity of copper oxide nanoparticles in human skin keratinocytes cells". International Journal of Toxicology, 32(4): 296-307, 2013.

[2] Arkhangelsky, E.; Denis K.; Vitaly G.; "Impact of chemical cleaning on properties and functioning of polyethersulfone membranes." Journal of Membrane Science, 305(1-2): 176-184, 2007.

[3] Barzin, J.; Madaeni, S. S.; Mirzadeh, H.; Mehrabzadeh, M.; "Effect of polyvinylpyrrolidone on morphology and performance of hemodialysis membranes prepared from polyether sulfone". Journal of Applied Polymer Science, 92(6): 3804-3813, 2004.

[4] Beyer, J.; Trannum, H.C.; Bakke, T.; Hodson, P.V.; Collier, T.K.; "Environmental elects of the Deepwater Horizon oil spill: A review". Marine Pollution Bulletin, 110: 28–51, 2016.

[5] Burgherr, P.; "In-depth analysis of accidental oil spills from tankers in the context of global spill trends from all sources". Journal of Hazardous Materials, 140(1-2): 245-256, 2007.

[6] Buskey, Edward J.; Helen K. W.; Andrew J. E.; "Impact of oil spills on marine life in the Gulf of Mexico: effects on plankton, nekton, and deep-sea benthos". Oceanography, 29(3): 174-181, 2016.

[7] Cho, D.O.; "The elects of the M/V Sea Prince accident on maritime safety management in Korea". Marine Policy, 31: 730–735, 2007.

[8] Dizaj, S. M.; Mennati, A.; Jafari, S.; Khezri, K.; Adibkia, K.; "Antimicrobial activity of carbon-based nanoparticles". Advanced pharmaceutical bulletin, 5(1): 19, 2015.

[9] El-Nahhal, M.; "Nanostructured copper oxide-cotton fibers: synthesis, characterization, and applications." International Nano Letters, 2: 1-5, 2012.

[10] Fayadh, Saeed M.;Asma H. M.; "Silver nanoparticles induced apoptosis in papillary and follicular thyroid carcinoma cells." Physics in Medicine, 14: 100056, 2022.

[11] Goh, P. S.; Ong, C. S.; Ismail, A. F.; "Applications of emerging nanomaterials for oily wastewater treatment". In Nanotechnology in Water and Wastewater Treatment. Elsevier, 101-113, 2019.

[12] Haider, Adawiya J.; Suaad S. S.; Asma H. M.; "A study of morphological, optical and gas sensing properties for pure and Ag doped SnO2 prepared by pulsed laser deposition (PLD)." Energy Procedia, 36: 776-787, 2013.

[13] Han, M.; Zhang, J.; Chu, W.; Chen, J.; Zhou, G. ; "Research progress and prospects of marine oily wastewater treatment: a review". Water, 11(12): 2517, 2019.
[14] Jamaly, S.; Giwa, A.;Hasan, S. W.; " Recent improvements in oily wastewater treatment Progress, challenges, and future opportunities" . Journal of Environmental Science, 37: 15-30, 2015.
[15] Jernelöv,; A. "The threats from oil spills: now, then, and in the future." Ambio, 39(5): 353-366, 2010.
[16] Jones, N.; Ray, B.; Ranjit, K. T.;Manna, A. C.; "Antibacterial activity of ZnO nanoparticle suspensions on a broad spectrum of microorganisms". FEMS Microbiology Letters, 279(1): 71-76, 2008.
[17] Marchese, J.; "Fouling behavior of polyethersulfone UF membranes made with different PVP." Journal of Membrane Science, 211(1): 1-11, 2003.
[18] Mirhosseini, M.; Barzegari Firouzabadi, F.; "Preparation of ZnO-Polystyerne Composite Films and Investigation of Antibacterial Properties of ZnOPolystyerne Composite Films". Iranian Journal of Pathology. 9(2):99-106, 2014.
[19] Parnas, Richard S.; "The adsorption of polyvinylpyrrolidone and polyethylene oxide onto chemically modified silica." Journal of Colloid and Interface Science, 129(2): 441-450, 1989.
[20] Pellegrin, B.; "Multi-scale analysis of hypochlorite induced PES/PVP ultrafiltration membranes degradation." Journal of Membrane Science, 447: 287-296, 2007.
[21] Peralta, J. R.; Zhao, L.; Lopez-Moreno, M. L.; de la Rosa, G.; Hong, J.; Gardea-Torresdey, J. L.; "Nanomaterials and the environment: a review for the biennium 2008–2010". Journal of Hazardous Materials, 186(1): 1-15, 2011.
[22] Sandstead, Harold H.; "Understanding zinc: recent observations and interpretations." The Journal of Laboratory and Clinical Medicine, 124(3): 322-327, 1994.
[23] Skocaj, M.; Filipic, M.; Petkovic, J.; Novak, S.; "Titanium dioxide in our everyday life; is it safe", Radiology and oncology, 45(4): 227-247,2011
[24] Soto, L. A.; Botello, A. V.; Licea-Durán, S.; Lizárraga-Partida, M. L.; Yáñez-Arancibia, A.; "The environmental legacy of the Ixtoc-I oil spill in Campeche Sound, southwestern Gulf of Mexico". Frontiers in Marine Science, 1: 57, 2014.
[25] Stuart, M. A.; Cohen, G. J.; Bijsterbosch, B. H.; "The adsorption of poly (vinyl pyrrolidone) onto silica. I. Adsorbed amount." Journal of Colloid and Interface Science, 90(2): 310-320, 1982.
[26] Van, D.; Bruggen, B.; "A review of pressure-driven membrane processes in wastewater treatment and drinking water production." Environmental Progress, 22(1): 46-56, 2003.
[27] Wan, M.; Zhao, H.; Peng, L.; Zou, X.; Zhao, Y.; Sun, L.; "Loading of Au/Ag bimetallic nanoparticles within and outside of the flexible SiO_2 electrospun nanofibers as highly sensitive, stable, repeatable substrates for versatile and trace SERS detection". Polymers, 12(12): 3008, 2020.
[28] Wang, H.; Yu, T.; Zhao, C.; Du, Q.; "Improvement of hydrophilicity and blood compatibility on polyethersulfone membrane by adding polyvinylpyrrolidone". Fibers and Polymers, 10: 1-5, 2009.
[29] Wienk, I. M.; "Chemical treatment of membranes of a polymer blend: mechanism of the reaction of hypochlorite with poly (vinyl pyrrolidone)." Journal of Polymer Science A: Polymer Chemistry, 33(1): 49-54, 1995.
[30] Wilczynski, M.; "Anti- microbial porcelain enamels". In 62nd Porcelain Enamel Institute Technical Forum: Ceramic Engineering and Science Proceedings, Hoboken, NJ, USA: John Wiley & Sons, 81-83, 2000.
[31] Wu, Z.; Gong, S.; Li, C., Zhang, Z.; Huang, W.; Meng, L.; He, Y.; "Novel water-soluble fluorescent polymer containing recognition units: Synthesis and interactions with PC12 cell". European Polymer Journal, 41(9): 1985-1992, 2005.